ATLAS CONF Note

ATLAS-CONF-2022-019

2nd April 2022

Comparison of inclusive and photon-tagged jet suppression in 5.02 TeV Pb+Pb collisions with ATLAS

The ATLAS Collaboration

This note presents a measurement of photon-tagged jet energy loss in the quark-gluon plasma, using 1.7 nb^{-1} of Pb+Pb data and 260 pb^{-1} of pp data, both at 5.02 TeV, with the ATLAS detector. The process $pp \rightarrow \gamma$+jet+X and its analogue in Pb+Pb events is measured in events with a $p_{\mathrm{T}}^{\gamma} > 50$ GeV isolated photon and reported as a function of jet transverse momentum (p_{T}). This selection results in a sample of jets with a steeply falling p_{T} distribution, similar to that for inclusive jets but with a different fraction of quark and gluon-initiated jets. The nuclear modification factor, R_{AA}, for photon-tagged jet production in Pb+Pb compared to pp is reported as a function of jet p_{T} and Pb+Pb event centrality, and compared to theoretical predictions. The R_{AA} for photon-tagged jets is measured to be significantly higher than that previously measured for inclusive jets, demonstrating that energy loss in the QGP is sensitive to the color-charge of the initiating parton.

ATLAS-CONF-2022-019
05 April 2022

1 Introduction

Ultra-relativistic collisions of heavy nuclei at the Large Hadron Collider (LHC) produce a hot, deconfined nuclear medium known as the quark-gluon plasma (QGP). The QGP exhibits surprising phenomena, such as a collective evolution that suggests it is a strongly-coupled fluid well-described by hydrodynamics [1]. The dense field of deconfined color charges which makes up the QGP is opaque to quarks and gluons attempting to pass through it. This results in hard-scattered partons suffering energy loss and a modification of their showering process as they traverse the QGP. This phenomenon is known as *jet quenching*, and results in a wide variety of experimental signatures [2].

A straightforward and broadly used signature of jet quenching is the suppression of jet production at fixed transverse momentum[1] (p_{T}) in Pb+Pb collisions compared to pp collisions. This is quantified by the nuclear modification factor, R_{AA}, which is defined as the ratio of the observed yield in Pb+Pb collisions to the expectation from an equivalent number of pp collisions, i.e. without jet quenching effects from the formation of a QGP. This expectation is calculated as the cross-section in pp collisions, scaled by the mean value of the nuclear thickness function in the corresponding Pb+Pb collisions, $\langle T_{\mathrm{AA}} \rangle$ [3]. The R_{AA} is thus defined as

$$R_{\mathrm{AA}} = \frac{1}{N_{\mathrm{evt}}} \frac{dN^{\mathrm{PbPb}}}{dp_{\mathrm{T}}^{\mathrm{jet}}} \Bigg/ \langle T_{\mathrm{AA}} \rangle \frac{d\sigma^{pp}}{dp_{\mathrm{T}}^{\mathrm{jet}}}, \tag{1}$$

where $\langle T_{\mathrm{AA}} \rangle$ can be considered to have the meaning of a per-Pb+Pb-event luminosity.

In central Pb+Pb collisions, the nuclei collide head on and create a large and long-lived volume of QGP. The developing showers of high-p_{T} partons interact strongly with the QGP, such that part of their momentum is transported to large angles with respect to the initial parton direction [4]. Thus, the total momentum in a fixed-size jet cone is decreased compared to the process with analogous initial kinematics occurring in pp collisions, and the jets can be thought of as migrating to lower p_{T} values in Pb+Pb events. Since the jet spectrum is steeply falling with p_{T}, this results in an R_{AA} below unity with a magnitude that depends on the local shape of the spectrum. In central Pb+Pb events at the LHC, the R_{AA} for inclusive jets is suppressed by approximately a factor of two at $p_{\mathrm{T}} \approx 100$ GeV [5–7].

A key aspect in the theoretical description of jet quenching is its sensitivity to the color charge of the initiating parton, i.e. whether that parton is a quark or gluon [8–18]. In pictures which describe the jet-medium interaction as proceeding dominantly by radiative emission (medium-induced gluon radiation by strong color charges), quarks and gluons are generally expected to lose energy in proportion to their color factors. Thus, gluon-initiated jets are expected to lose significantly more energy than quark-initiated ones. At LHC energies, inclusive jet production is dominated by gluon-initiated jets. On the other hand, jets produced in association with an isolated photon or electroweak (EW) boson, for example through Compton scattering ($gq \to q\gamma$), are significantly more likely to be initiated by a quark compared to inclusive jets at the same p_{T}. Importantly, the kinematics of the colorless photon or EW boson are not significantly modified by the QGP [19]. Thus ATLAS has used an isolated photon or Z boson as a tag on the initial

[1] ATLAS uses a right-handed coordinate system with its origin at the nominal interaction point (IP) in the centre of the detector and the z-axis along the beam pipe. The x-axis points from the IP to the centre of the LHC ring, and the y-axis points upward. Cylindrical coordinates (r, ϕ) are used in the transverse plane, ϕ being the azimuthal angle around the z-axis. The pseudorapidity is defined in terms of the polar angle θ as $\eta = -\ln\tan(\theta/2)$.

parton kinematics before jet quenching to study how the resulting jet [20] or hadron [21, 22] distributions are modified in particular selections of boson p_{T}.

This note presents a measurement of the process $pp(\text{or } NN) \rightarrow \gamma\text{+jet+}X$, as a function of jet p_{T}. Events are required to have an isolated photon with $p_{\mathrm{T}}^{\gamma} > 50$ GeV and $|\eta| < 2.37$ (excluding the region $1.37 < |\eta| < 1.52$). All jets with $|\eta| < 2.8$ and $p_{\mathrm{T}}^{\mathrm{jet}} > 50$ GeV in the azimuthal hemisphere opposite the photon ($\Delta\phi > \pi/2$) are included in the measurement. The measurement is performed using 260 pb^{-1} and 1.7 nb^{-1} of pp and Pb+Pb collisions at 5.02 TeV, respectively, recorded with the ATLAS detector at the LHC. This requirement selects a set of jets with a steeply falling p_{T} distribution similar to that for inclusive jets, but with a significantly larger quark-initiated fraction. Thus, comparing the R_{AA} for photon-tagged jets reported in this note to that for inclusive jets measured in Ref. [5] allows for a controlled examination of the impact of the initiating parton's color-charge on jet energy loss.

2 ATLAS detector

The ATLAS experiment [23] at the LHC is a multipurpose particle detector with a forward–backward symmetric cylindrical geometry and a near 4π coverage in solid angle. Its inner tracking detector is surrounded by a thin superconducting solenoid providing a 2 T axial magnetic field, and electromagnetic and hadron calorimeters. The inner tracking detector covers the pseudorapidity range $|\eta| < 2.5$. It consists of silicon pixel, silicon microstrip, and transition radiation tracking detectors. Lead/liquid-argon (LAr) sampling calorimeters provide electromagnetic (EM) energy measurements with high granularity. A steel/scintillator-tile hadron calorimeter covers the central pseudorapidity range ($|\eta| < 1.7$). The endcap and forward regions are instrumented with LAr calorimeters for both the EM and hadronic energy measurements up to $|\eta| = 4.9$. A zero-degree calorimeter (ZDC) is situated at $|\eta| > 8.3$. It is composed of alternating layers of quartz rods and tungsten plates and is mostly sensitive to spectator neutrons from fragmenting nuclei in Pb+Pb collisions.

A two-level trigger system is used to select events [24]. The first-level trigger is implemented in hardware and uses a subset of the detector information to accept events at a rate below 100 kHz. This is followed by a software-based trigger that reduces the accepted event rate to 1 kHz on average depending on the data-taking conditions. An extensive software suite [25] is used in the reconstruction and analysis of real and simulated data, in detector operations, and in the trigger and data acquisition systems of the experiment.

3 Event and data selection

Events in data are selected for analysis using triggers requiring a reconstructed photon with p_{T} above 35 GeV (20 GeV) in pp (Pb+Pb) collisions [24, 26]. The trigger sampled the full luminosity which corresponds to 260 pb^{-1} of pp data in 2017 and 1.7 nb^{-1} of Pb+Pb data in 2018, and is fully efficient for the photon selection used in the analysis below. Events are required to have a reconstructed vertex and to pass detector and data-quality requirements.

The Pb+Pb event centrality is characterized by the sum of the transverse energy in the forward calorimeters, $\Sigma E_{\mathrm{T}}^{\mathrm{FCal}}$. Events in different ranges of $\Sigma E_{\mathrm{T}}^{\mathrm{FCal}}$ are associated with an underlying geometric configuration according to a Monte Carlo (MC) Glauber simulation [3, 27]. This analysis uses three centrality intervals

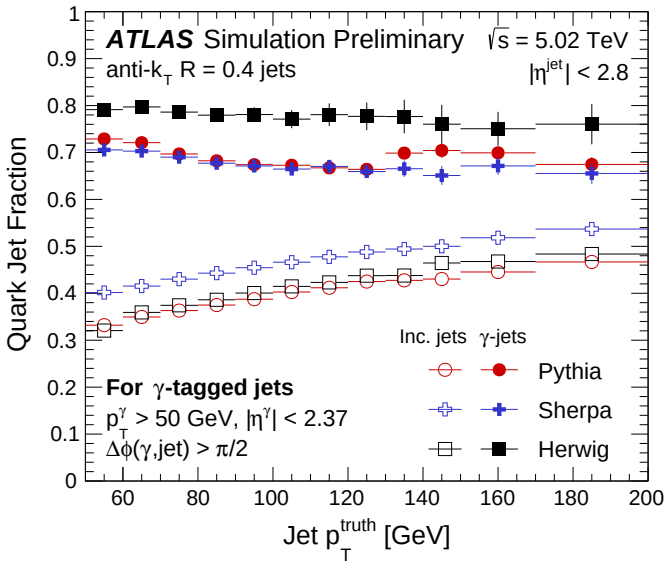

Figure 1: Fraction of photon-tagged jets (filled markers) and inclusive jets (open markers) initiated by a quark, as a function of $p_{\mathrm{T}}^{\mathrm{jet}}$, in the PYTHIA (red), HERWIG (black), and SHERPA (blue) event generators.

corresponding to the following fractions of the $\Sigma E_{\mathrm{T}}^{\mathrm{FCal}}$ distribution in minimum-bias events: 0–10% ("central" events, with a large nuclear overlap), 10–30%, and 30–80% ("peripheral" events).

This analysis uses samples of MC-simulated events to evaluate the performance of the photon and jet reconstruction and to correct the measured distributions for detector effects. The main MC sample corresponding to the pp data consists of PYTHIA8 [28] events, produced with the A14 [29] tune and NNPDF 2.3 LO [30] parton distribution function (PDF) set. As alternatives, photon+jet events are also produced using two additional generators. The SHERPA 2.2.4 [31, 32] generator was run at next-to-leading order with the NNPDF 3.0 NNLO [33] PDF set to produce a photon plus up to three other partons. The HERWIG 7.2 [34] generator was run at leading order with the MMHT2014lo [35] PDF set, and separate samples for direct and fragmentation photons. The three sets of events are simulated [25] within ATLAS using GEANT4 [36] and are digitized and reconstructed in a manner identical to that in data.

The fraction of quark-initiated jets in the photon-tagged jet sample in simulation is shown in Figure 1. This fraction is 0.7–0.8 over the measured $p_{\mathrm{T}}^{\mathrm{jet}}$ range, which is significantly higher than the quark-initiated jet fraction of 0.3–0.5 for inclusive jets in the same kinematic range.

To simulate photon+jet events in Pb+Pb data, the above events are overlaid at the hit level with a sample of Pb+Pb data events recorded with minimum-bias and central-event triggers, and the combination was reconstructed as a single event. These "Pb+Pb data overlay" events are reweighted to match the observed $\Sigma E_{\mathrm{T}}^{\mathrm{FCal}}$ distribution for photon+jet events in Pb+Pb data. In this way, the features of the Pb+Pb underlying event (UE) in the simulated samples are identical to those in real Pb+Pb data.

4 Analysis

Photons are reconstructed following the method used previously in Pb+Pb collisions [20, 22], which applies the procedure used in pp collisions [37] after an event-by-event estimation and subtraction of the UE contribution to the energy deposited in each calorimeter cell [38]. Photon candidates are required to pass "tight" shower shape cuts designed to reject those arising from neutral meson decays and the start of hadronic showers in the electromagnetic calorimeter [39]. In pp collisions, photons are further required to be isolated by requiring that the sum of the transverse energy in calorimeter cells within $\Delta R < 0.3$ (not including the contribution from the photon itself) is less than 3 GeV. In Pb+Pb collisions, the UE fluctuations within the isolation cone result in a substantial broadening of the isolation E_{T} distribution. Thus, in Pb+Pb collisions, the isolation energy requirement is centrality-dependent and is chosen so that its efficiency for prompt photons is 90%, as determined in simulation. This upper limit is 10 GeV in 0–10% Pb+Pb events, but quickly decreases and converges to the pp value in peripheral events.

Jets are reconstructed following the procedure used in Pb+Pb collisions [5, 38], which is summarized here. The anti-k_t algorithm [40, 41] with cone parameter $R = 0.4$ is applied to cells in all calorimeter layers, evaluated at the electromagnetic energy scale, and regrouped into $\Delta\eta \times \Delta\phi = 0.1 \times \pi/32$ logical towers. After the initial jet-finding, the contribution to the energy deposited in towers by the UE is estimated on an event-by-event basis, allowing for the variation of the UE as a function of η and ϕ (the latter arising from the global collective flow in Pb+Pb collisions). Information from towers within $\Delta R < 0.4$ of jet candidates is excluded to avoid biasing the UE estimate. The tower kinematics are updated to subtract the estimated UE contribution, and the UE procedure is iterated using a better-defined set of jets to define the exclusion regions. The resulting set of jet kinematics is corrected using p_{T}- and η-dependent factors, determined in simulation, to account for the response of the calorimeter to jets [42]. An additional correction for the absolute response in data is based on *in situ* studies of jets recoiling against photons, Z bosons, and jets in other regions of the calorimeter in pp collisions [20]. This calibration is followed by a "cross-calibration" which relates the jet energy scale (JES) of jets reconstructed by the procedure outlined above to that in 13 TeV pp collisions [43].

The signal definition for this measurement is the $p_{\mathrm{T}}^{\mathrm{jet}}$ distribution of $R = 0.4$ jets with $p_{\mathrm{T}}^{\mathrm{jet}} > 50$ GeV which are $\Delta\phi > \pi/2$ from a $p_{\mathrm{T}}^{\gamma} > 50$ GeV isolated photon, with all candidate jets in a given event included in the measurement. In the analysis, the two-dimensional yield $(p_{\mathrm{T}}^{\gamma}, p_{\mathrm{T}}^{\mathrm{jet}})$ is constructed for photons and their associated jets, but using thresholds of 40 GeV on the photon and jet p_{T}, to allow for the correction of bin migration effects (discussed below).

The initial $(p_{\mathrm{T}}^{\gamma}, p_{\mathrm{T}}^{\mathrm{jet}})$ yield in Pb+Pb collisions contains jets which do not arise from the same hard scattering as the photon, but rather from an unrelated nucleon–nucleon scattering, or from jets which are reconstructed from the localized fluctuations of the UE. This combinatoric contribution is estimated through a "mixing" technique in which the high-p_{T} photons in data are correlated with jets in minimum-bias Pb+Pb events that match the overall properties of the original, photon-containing event. These matched properties include the $\Sigma E_{\mathrm{T}}^{\mathrm{FCal}}$, event plane angle, and z vertex position. The resulting combinatoric jet contribution is observed to be flat in $\Delta\phi$, as expected for unrelated pairs. For the lowest $p_{\mathrm{T}}^{\mathrm{jet}}$ values in the most central events, the background contribution is approximately half of the total yield, but this fraction falls very quickly with increasing $p_{\mathrm{T}}^{\mathrm{jet}}$ or in less central events. The contribution is statistically subtracted from the initial yields.

Even after the photon identification and isolation conditions above are applied to data, the pre-selected photons still include a considerable contribution of backgrounds, dominantly from neutral hadron decays (e.g. $\pi^0, \eta \to \gamma\gamma$). These decay photons may be reconstructed as a single cluster which passes the "tight"

identification and the isolation conditions. Thus, the photon-associated jet yields contain a contribution from, e.g. π^0-associated jet yields. To correct for this, the purity of prompt, isolated photons in the selected data sample is determined using a data-driven, double-sideband method widely used in ATLAS photon measurements [44–47], separately for each selection in event centrality and p_{T}^{γ}. The purity has a minimum of $\approx 75\%$ in central Pb+Pb events at the lowest p_{T}^{γ} values, but then increases quickly with p_{T}^{γ} and in more peripheral Pb+Pb or pp events to a plateau of $\approx 95\%$. The shape of the $p_{\mathrm{T}}^{\mathrm{jet}}$ contribution from this background is determined by performing the same analysis but using an inverted signal selection on the photon. This selection requires the photon to fail several shower shape requirements in a way that is designed to greatly enhance the neutral hadron background. Finally, the background level is scaled according to the purity in each p_{T}^{γ} and centrality selection, and statistically subtracted.

To correct for the bin-to-bin migration in p_{T}^{γ} and $p_{\mathrm{T}}^{\mathrm{jet}}$ arising from the finite detector resolution, a two-dimensional unfolding procedure on the background-subtracted $(p_{\mathrm{T}}^{\gamma}, p_{\mathrm{T}}^{\mathrm{jet}})$ yields is used. The Pythia8 simulation samples are used to generate independent response matrices for pp events and for each centrality range in Pb+Pb events, after reweighting the $p_{\mathrm{T}}^{\mathrm{jet}}$ distributions in simulation to match those measured in data. The iterative Bayesian method [48] is used with the RooUnfold software package [49]. The number of iterations used in the unfolding is determined by minimizing the quadrature sum of the total statistical uncertainty and the differences in the unfolded distribution between consecutive iterations. The unfolding procedure also accounts for the finite reconstruction efficiency of photons, which is $\approx 70\%$ at low-p_{T}^{γ} in central Pb+Pb events, but rises quickly with p_{T}^{γ} and in more peripheral events to a plateau of $\approx 85\%$. When tested in simulation, this unfolding procedure leads to an excellent recovery of the original truth-level distribution.

5 Systematic Uncertainty

The main sources of systematic uncertainty in this measurement are those associated with the photon, jet, and unfolding components. For each source described below, the entire analysis is repeated with a given variation, and the change in the results is taken as the corresponding uncertainty. These individual uncertainties are treated as independent and added in quadrature to determine the full uncertainties.

The photon measurement includes several uncertainty components. First, the reconstructed energy of photons in simulation is varied according to the uncertainties for photon energy scale and resolution [50]. Second, the reconstructed shower shape variables used to identify photons are varied in simulation [39]. Third, the isolation and identification sideband boundaries used in purity determination are varied in a manner similar to that in Refs. [20, 22]. Fourth, the difference between using the nominal purity values and the results of a smooth fit to those values is considered.

For the jet-related uncertainties, the reconstructed jet energy in simulation is varied according to the uncertainties on the jet energy scale (JES) and resolution (JER). As in other Run-2 heavy-ion jet measurements [4, 5, 20, 22, 51, 52], the JES uncertainties have four main components: 1) a centrality-independent baseline component determined from *in situ* studies of the calorimeter response for jets reconstructed following the procedure used in 13 TeV pp collisions [53, 54]; 2) a centrality-independent component accounting for the relative energy scale difference between the heavy-ion jet reconstruction in this analysis and that used for 13 TeV pp collisions [43]; 3) a component which accounts for potential inaccuracies in the relative abundances of jets initiated by quarks and gluons, and of their different calorimetric response, in simulation. This uncertainty was evaluated by using the Herwig instead of

PYTHIA8 simulation samples; 4) a centrality-dependent component accounting for a different structure and possibly a different detector response of jets in Pb+Pb collisions that is not modeled in simulation. This uncertainty is determined by the method used for 2015 and 2011 data [43] that compares the calorimeter p_{T} with the p_{T} sum of the charged particles within the jet between data and simulation. For the JER uncertainty, the reconstructed $p_{\mathrm{T}}^{\mathrm{jet}}$ in simulation is smeared by a factor evaluated using an *in situ* technique in 13 TeV pp data [55, 56], and by an additional contribution to account for the differences between the heavy-ion jet reconstruction and that in the 13 TeV pp data.

Two uncertainties associated with the unfolding procedure were evaluated. First, the impact of a different prior in the response matrices was determined by not applying the reweighting factors to account for the difference in the distributions between data and simulation. Second, a resampling study was used to determine the impact on the results from the limited size of the simulated samples, which were added to the statistical uncertainties.

Finally, there are uncertainties in the overall normalization of the measurements. For the pp cross-section, these arise from the luminosity of the pp data and are estimated to be 1.6% using the beam separation scan analysis methods similar to that in Ref. [57]. For the $1/\langle T_{\mathrm{AA}}\rangle$-scaled yields in Pb+Pb collisions, the uncertainties are determined by adjusting the parameters in the Glauber analysis [3, 27], and vary from 0.5% to 2.8% in central to peripheral collisions, respectively.

Uncertainty sources which are correlated between Pb+Pb and pp collisions, which include most of the jet- and photon-related uncertainties, typically cancel to a large degree in the R_{AA} ratio. The most significant uncorrelated uncertainties are the centrality-dependent JES and unfolding ones. For the cross-section measurements, the jet energy scale uncertainties are dominant in almost the entire phase space. For the R_{AA} measurements, the jet energy scale (photon purity) uncertainties are dominant at $p_{\mathrm{T}}^{\mathrm{jet}} > 80$ GeV for 0–10% and 10–30% centrality bins (30–80% centrality bin). At $p_{\mathrm{T}}^{\mathrm{jet}} < 80$ GeV, the unfolding uncertainties are dominant for the R_{AA} measurements in all centrality bins. In comparisons of the R_{AA} reported in this note to that measured for inclusive jets [5], the uncertainties are treated as uncorrelated.

6 Results

This section presents the measurement of the cross-section $pp \to \gamma + \mathrm{jet} + X$ and its equivalent in Pb+Pb collisions, as a function of $p_{\mathrm{T}}^{\mathrm{jet}}$ for jets, with the full kinematic selection given in Section 1. Figure 2 shows the measured cross-section for photon-tagged jet production in pp collisions, compared with the same quantity in three event generators. The truth-level photons in the generators are required to be isolated by requiring that the sum of all the final state particles, excluding the photon itself, within $\Delta R < 0.3$ is less than 5 GeV. All three generators are compatible with the data within uncertainties in the low $p_{\mathrm{T}}^{\mathrm{jet}}$ region ($p_{\mathrm{T}}^{\mathrm{jet}} <$ 100 GeV) but have a higher cross-section than the data at higher $p_{\mathrm{T}}^{\mathrm{jet}}$. In a similar measurement at 7 TeV, these event generators were also found to have difficulty to describe the relative shape at high-$p_{\mathrm{T}}^{\mathrm{jet}}$ [58].

Figure 3 presents the cross-section in pp collisions and the per-event yields in Pb+Pb collisions with three different centrality selections, each scaled by $1/\langle T_{\mathrm{AA}}\rangle$ for the given selection. The photon-tagged jet cross-section in pp collisions is compared to the cross-section for inclusive jets from Ref. [5]. The bottom panel shows the ratio of cross-sections between the photon-tagged and inclusive jets in pp collisions. The ratio rises by a factor of four over the $p_{\mathrm{T}}^{\mathrm{jet}}$ range, indicating that while the $p_{\mathrm{T}}^{\mathrm{jet}}$ spectrum for photon-tagged jets is steeply falling, it is somewhat harder than that for inclusive jets.

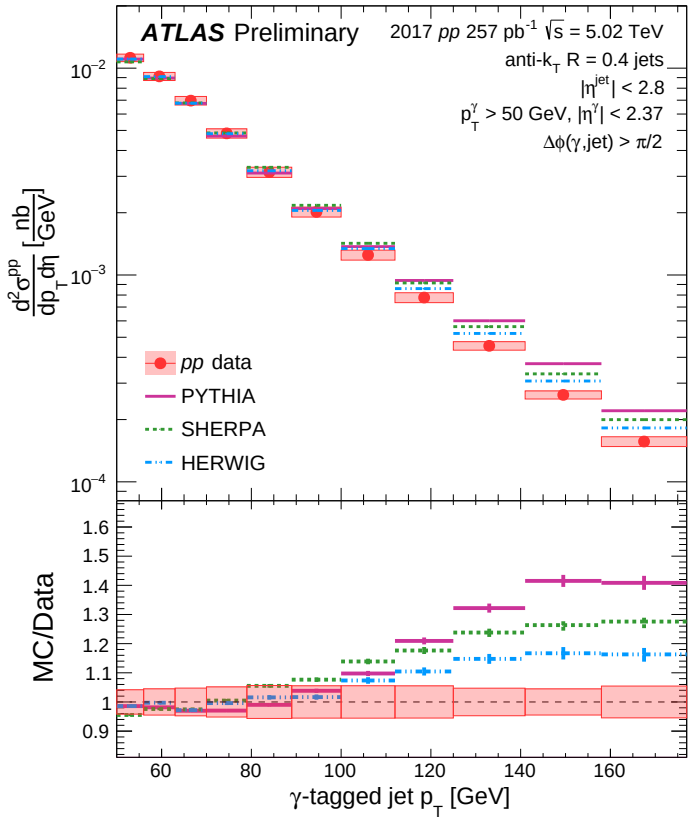

Figure 2: Top: Cross-section of photon-tagged jets as a function of $p_{\mathrm{T}}^{\mathrm{jet}}$ in pp data (red) is compared to PYTHIA (purple), SHERPA (green), and HERWIG (blue) generators. The statistical uncertainties are smaller than the marker size, and the total systematic uncertainties for data are shown as boxes. For the generators only the central values are shown without systematic uncertainties. Bottom: The ratio of the cross-section between the generators and the data.

Figure 4 presents the nuclear modification factor, R_{AA}, for photon-tagged jets in the three Pb+Pb centrality selections. The R_{AA} is significantly below unity, with the R_{AA} in more central events systematically lower than in peripheral events. In the region $p_{\mathrm{T}}^{\mathrm{jet}} > 80$ GeV the R_{AA} in all centralities slowly rises with $p_{\mathrm{T}}^{\mathrm{jet}}$. This behavior is similar to that observed for the R_{AA} of inclusive jets [5], and may indicate that the typical fraction of energy lost decreases with increasing jet p_{T}. In the region $p_{\mathrm{T}}^{\mathrm{jet}} < 80$ GeV the R_{AA} rises as $p_{\mathrm{T}}^{\mathrm{jet}}$ decreases, an effect that may arise from the changing shape of the photon-tagged $p_{\mathrm{T}}^{\mathrm{jet}}$ distribution as it approaches the photon p_{T}^{γ} threshold of 50 GeV.

In 0–10% Pb+Pb events, the R_{AA} for photon-tagged jets is approximately 0.6 at $p_{\mathrm{T}}^{\mathrm{jet}} = 100$ GeV, which is significantly larger than the R_{AA} of approximately 0.45 for inclusive jets at the same $p_{\mathrm{T}}^{\mathrm{jet}}$ and Pb+Pb centrality. As motivated above, one important difference between the two samples of jets (photon-tagged and inclusive) is the different quark/gluon fraction, as shown in Figure 1. However, a difference in the R_{AA} for these processes could potentially arise for two additional reasons unrelated to the color charge dependence of energy loss. First, as discussed above, the photon-tagged $p_{\mathrm{T}}^{\mathrm{jet}}$ distribution is somewhat

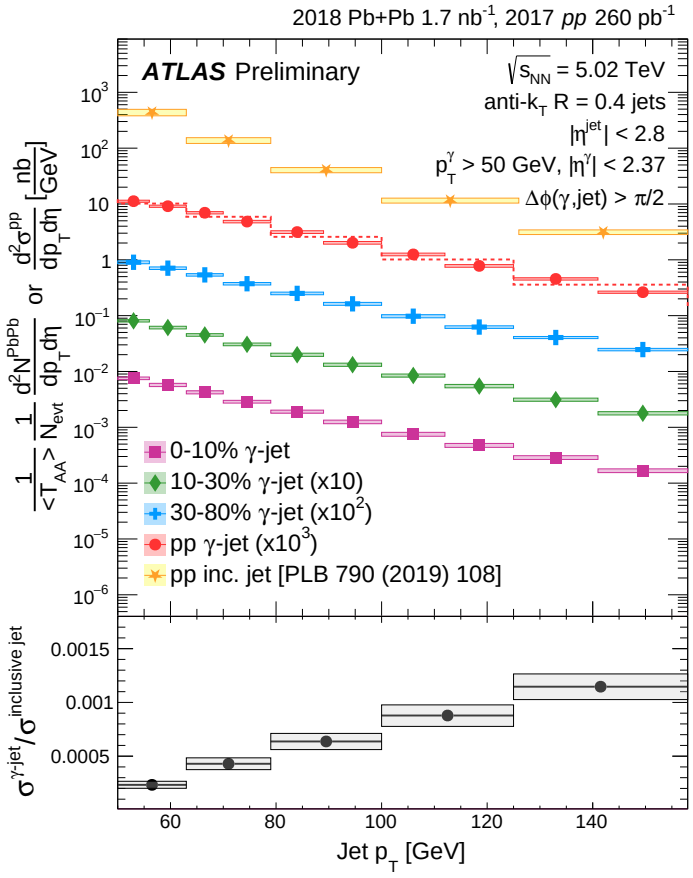

Figure 3: Top: Per-event yields of photon-tagged jets in 0–10% (purple), 10–30% (green), and 30–80% (blue) Pb+Pb events, scaled by $1/\langle T_{\mathrm{AA}}\rangle$, and the cross-section in pp events (red). The spectra are vertically displaced by multiplicative factors shown in the legend for clarity. The cross-section for inclusive jets in pp collisions [5] is shown in yellow markers. The statistical uncertainties are smaller than the marker size, and the total systematic uncertainties are shown as boxes. The dashed red line is the cross section for photon-tagged jets in pp collisions, rebinned to match the binning for inclusive jets. Bottom: The ratio of cross sections between photon-tagged jets and inclusive jets in pp collisions.

harder than that for inclusive jets. For a fixed amount of energy loss, a harder spectrum results in a higher R_{AA}. Within a simple model of fractional energy loss, the difference in the spectral shapes could cause the photon-tagged jet R_{AA} to be larger by 10% even if energy loss were independent of color charge. Second, the production rate of photon+jet processes is known to be modestly suppressed in Pb+Pb collisions compared to pp collisions, due to the modification of parton densities in nuclei. For the case of photon+jet production, this mostly arises from the decreased number of valence up quarks, which have a higher absolute electric charge, compared to down quarks [59] in nuclei compared to protons. Such "isospin"-dependent suppression has been directly observed by ATLAS for photons in p+Pb collisions [60] and $W^{\pm}$ bosons in Pb+Pb collisions [61], and may suppress the photon-tagged jet R_{AA} by 5–10%, depending on the exact kinematics and photon origin (for a discussion, see Ref. [10]). Thus, these two effects are expected to have opposite sign and similar magnitude. Therefore, while the significant difference in the photon-tagged and inclusive jet R_{AA} arises dominantly from the color charge dependence of energy loss, it is necessary to

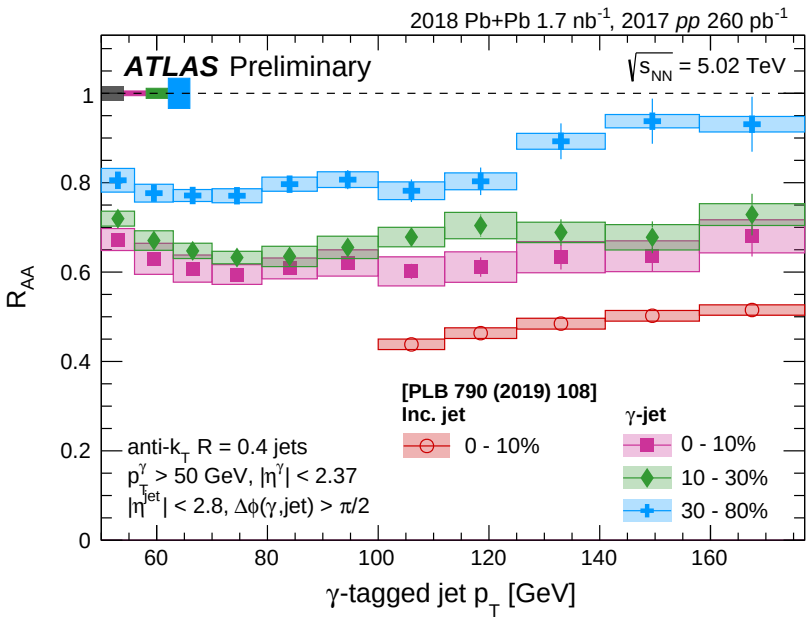

Figure 4: R_{AA} for photon-tagged jets as a function of $p_{\mathrm{T}}^{\mathrm{jet}}$ in 0–10% (purple), 10–30% (green), and 30–80% (blue) Pb+Pb collisions. The inclusive jet R_{AA} in 0–10% events (red) from Ref. [5] is shown for comparison. Statistical and systematic uncertainties are indicated by vertical bars and shaded boxes, respectively. The coloured and grey shaded boxes at $R_{\mathrm{AA}} = 1$ represent fractional $1/\langle T_{\mathrm{AA}} \rangle$ and pp luminosity uncertainties, respectively, which both affect the overall normalisation of the result.

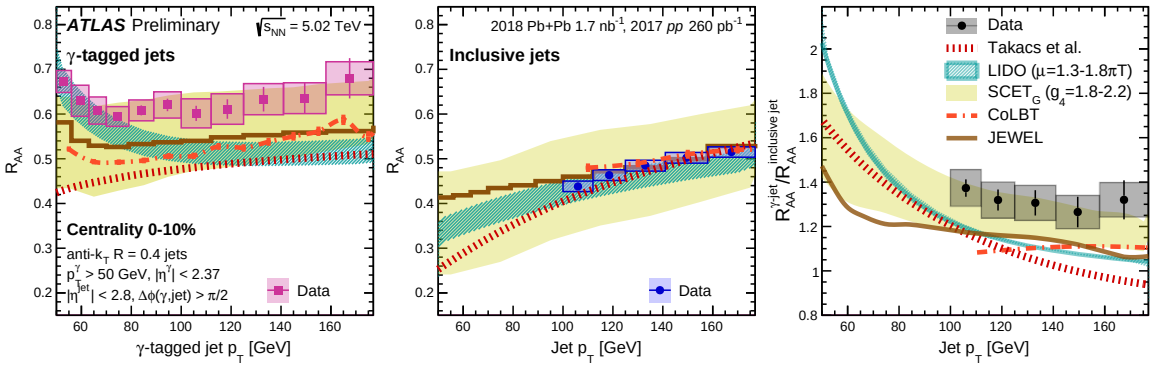

Figure 5: Comparison of R_{AA} for photon-tagged jets (left), inclusive jets (middle), and their ratio (right) in 0–10% Pb+Pb events to various theoretical predictions (see text). The vertical bars and shaded boxes on the data points indicate the statistical and total systematic uncertainties.

compare them to theoretical calculations which include the two effects described above to quantitatively constrain the magnitude of this physics effect.

The data were compared to the following five state-of-the-art theoretical calculations. The calculation by Takacs et al. [9, 10] includes resummation of energy loss effects from hard, vacuum-like emissions occurring in the medium and modeling of soft energy flow and recovery at the jet cone. The calculations in Ref. [11–13] are based on a Linearized Boltzmann Equation with diffusion model (LIDO), with the width of the band in the Figures corresponding to the range of jet-medium coupling cutoff parameter $\mu = (1.55 \pm 0.25)\pi T$. A perturbative calculation is performed within the framework of soft-collinear effective field theory with Glauber gluons ($\mathrm{SCET_G}$) in the soft-gluon-emission (energy-loss) limit [14–16], with the width of the band in the Figures corresponding to the range of jet-medium coupling $g = 2.0 \pm 0.2$. The CoLBT predictions [17] are a Linear Boltzmann Transport (LBT) model, which includes elastic and inelastic processes based on perturbative quantum chromodynamics (QCD) for both jet shower and recoil medium partons as they propagate through a QGP. Finally, JEWEL is an MC event generator which simulates QCD jet evolution in heavy-ion collisions, including radiative and elastic energy loss processes, and configured to include medium recoils [62].

The left panel of Figure 5 compares the photon-tagged jet R_{AA} in 0–10% Pb+Pb events with these predictions. The data are generally higher than the predictions, but are compatible with the $\mathrm{SCET_G}$ calculation using a lower value of g. The middle panel compares the inclusive jet R_{AA} in 0–10% Pb+Pb events from Ref. [5] with the predictions. All calculations describe the inclusive jet data very well, which may arise from tuning free parameters to this previously available dataset. The right panel compares the ratio of the R_{AA} between photon-tagged jets and inclusive jets, $R_{\mathrm{AA}}^{\gamma-\mathrm{jet}}/R_{\mathrm{AA}}^{\text{inclusive jet}}$. All theory calculations predict a $R_{\mathrm{AA}}^{\gamma-\mathrm{jet}}/R_{\mathrm{AA}}^{\text{inclusive jet}}$ value above unity, which evolves with $p_{\mathrm{T}}^{\mathrm{jet}}$. The data points are above most of the calculations but are compatible with the $\mathrm{SCET_G}$ calculation within uncertainties. In general, the agreement of the predictions with the inclusive jet measurement, but the different predictions for the photon-tagged jet case highlights the ability of this data to provide new constraints on the color charge dependence of energy loss in models.

7 Conclusion

This note presents a measurement of photon-tagged jet production in Pb+Pb and pp collisions at 5.02 TeV with the ATLAS detector. The cross-section of jets produced opposite in azimuth to a $p_{\mathrm{T}}^{\gamma} > 50$ GeV isolated photon is reported as a function of $p_{\mathrm{T}}^{\mathrm{jet}}$. This selection results in a sample of jets with a steeply falling p_{T} distribution, similar to that for inclusive jets, but with a significantly higher fraction of quark-initiated jets. The nuclear modification factor, R_{AA}, for photon-tagged jets is found to be suppressed below unity in a way that varies with centrality but only weakly in the reported $p_{\mathrm{T}}^{\mathrm{jet}}$ range. The photon-tagged jet R_{AA} is significantly higher than that for inclusive jets at the same $p_{\mathrm{T}}^{\mathrm{jet}}$ and centrality, indicating that parton energy loss is sensitive to the color charge of the initiating parton. The results are compared to a variety of theoretical calculations, which tend to overpredict the amount of energy loss for this quark-dominated jet sample.

References

[1] W. Busza, K. Rajagopal and W. van der Schee,
Heavy Ion Collisions: The Big Picture, and the Big Questions,
Ann. Rev. Nucl. Part. Sci. **68** (2018) 339, arXiv: 1802.04801 [hep-ph] (cit. on p. 2).

[2] L. Cunqueiro and A. M. Sickles, *Studying the QGP with Jets at the LHC and RHIC*, (2021),
arXiv: 2110.14490 [nucl-ex] (cit. on p. 2).

[3] M. L. Miller, K. Reygers, S. J. Sanders and P. Steinberg,
Glauber modeling in high energy nuclear collisions, Ann. Rev. Nucl. Part. Sci. **57** (2007) 205,
arXiv: nucl-ex/0701025 (cit. on pp. 2, 3, 7).

[4] ATLAS Collaboration, *Measurement of angular and momentum distributions of charged particles within and around jets in Pb+Pb and pp collisions at* $\sqrt{s_{NN}} = 5.02$ *TeV with the ATLAS detector*,
Phys. Rev. C **100** (2019) 064901, arXiv: 1908.05264 [hep-ex] (cit. on pp. 2, 6),
Erratum: Phys. Rev. C **101** (2019) 059903.

[5] ATLAS Collaboration, *Measurement of the nuclear modification factor for inclusive jets in Pb+Pb collisions at* $\sqrt{s_{NN}} = 5.02$ *TeV with the ATLAS detector*, Phys. Lett. B **790** (2019) 108,
arXiv: 1805.05635 [hep-ex] (cit. on pp. 2, 3, 5–11).

[6] CMS Collaboration,
First measurement of large area jet transverse momentum spectra in heavy-ion collisions,
JHEP **05** (2021) 284, arXiv: 2102.13080 [hep-ex] (cit. on p. 2).

[7] ALICE Collaboration,
Measurements of inclusive jet spectra in pp and central Pb-Pb collisions at $\sqrt{s_{\mathrm{NN}}} = 5.02$ *TeV*,
Phys. Rev. C **101** (2020) 034911, arXiv: 1909.09718 [nucl-ex] (cit. on p. 2).

[8] M. Spousta and B. Cole, *Interpreting single jet measurements in Pb + Pb collisions at the LHC*,
Eur. Phys. J. C **76** (2016) 50, arXiv: 1504.05169 [hep-ph] (cit. on p. 2).

[9] Y. Mehtar-Tani, D. Pablos and K. Tywoniuk,
Cone-Size Dependence of Jet Suppression in Heavy-Ion Collisions,
Phys. Rev. Lett. **127** (2021) 252301, arXiv: 2101.01742 [hep-ph] (cit. on pp. 2, 11).

[10] A. Takacs and K. Tywoniuk, *Quenching effects in the cumulative jet spectrum*, JHEP **10** (2021) 038,
arXiv: 2103.14676 [hep-ph] (cit. on pp. 2, 9, 11).

[11] W. Ke, Y. Xu and S. A. Bass, *Modified Boltzmann approach for modeling the splitting vertices induced by the hot QCD medium in the deep Landau-Pomeranchuk-Migdal region*,
Phys. Rev. C **100** (2019) 064911, arXiv: 1810.08177 [nucl-th] (cit. on pp. 2, 11).

[12] W. Ke, Y. Xu and S. A. Bass,
Linearized Boltzmann-Langevin model for heavy quark transport in hot and dense QCD matter,
Phys. Rev. C **98** (2018) 064901, arXiv: 1806.08848 [nucl-th] (cit. on pp. 2, 11).

[13] W. Ke and X.-N. Wang, *QGP modification to single inclusive jets in a calibrated transport model*,
JHEP **05** (2021) 041, arXiv: 2010.13680 [hep-ph] (cit. on pp. 2, 11).

[14] Z.-B. Kang, I. Vitev and H. Xing, *Vector-boson-tagged jet production in heavy ion collisions at energies available at the CERN Large Hadron Collider*, Phys. Rev. C **96** (2017) 014912,
arXiv: 1702.07276 [hep-ph] (cit. on pp. 2, 11).

[15] H. T. Li and I. Vitev, *Inclusive heavy flavor jet production with semi-inclusive jet functions: from proton to heavy-ion collisions*, JHEP **07** (2019) 148, arXiv: 1811.07905 [hep-ph] (cit. on pp. 2, 11).

[16] H. T. Li and I. Vitev, *Jet charge modification in dense QCD matter*, Phys. Rev. D **101** (2020) 076020, arXiv: 1908.06979 [hep-ph] (cit. on pp. 2, 11).

[17] Y. He et al., *Interplaying mechanisms behind single inclusive jet suppression in heavy-ion collisions*, Phys. Rev. C **99** (2019) 054911, arXiv: 1809.02525 [nucl-th] (cit. on pp. 2, 11).

[18] J. Brewer, J. Thaler and A. P. Turner, *Data-driven quark and gluon jet modification in heavy-ion collisions*, Phys. Rev. C **103** (2021) L021901, arXiv: 2008.08596 [hep-ph] (cit. on p. 2).

[19] CMS Collaboration, *The production of isolated photons in PbPb and pp collisions at* $\sqrt{s_{NN}} = 5.02$ *TeV*, JHEP **07** (2020) 116, arXiv: 2003.12797 [hep-ex] (cit. on p. 2).

[20] ATLAS Collaboration, *Measurement of photon-jet transverse momentum correlations in* 5.02 *TeV Pb+Pb and pp collisions with ATLAS*, Phys. Lett. B **789** (2019) 167, arXiv: 1809.07280 [hep-ex] (cit. on pp. 3, 5, 6).

[21] ATLAS Collaboration, *Medium-Induced Modification of Z-Tagged Charged Particle Yields in Pb+Pb Collisions at* 5.02 *TeV with the ATLAS Detector*, Phys. Rev. Lett. **126** (2021) 072301, arXiv: 2008.09811 [hep-ex] (cit. on p. 3).

[22] ATLAS Collaboration, *Comparison of Fragmentation Functions for Jets Dominated by Light Quarks and Gluons from pp and Pb+Pb Collisions in ATLAS*, Phys. Rev. Lett. **123** (2019) 042001, arXiv: 1902.10007 [hep-ex] (cit. on pp. 3, 5, 6).

[23] ATLAS Collaboration, *The ATLAS Experiment at the CERN Large Hadron Collider*, JINST **3** (2008) S08003 (cit. on p. 3).

[24] ATLAS Collaboration, *Performance of the ATLAS trigger system in 2015*, Eur. Phys. J. C **77** (2017) 317, arXiv: 1611.09661 [hep-ex] (cit. on p. 3).

[25] ATLAS Collaboration, *The ATLAS Collaboration Software and Firmware*, ATL-SOFT-PUB-2021-001, 2021, URL: https://cds.cern.ch/record/2767187 (cit. on pp. 3, 4).

[26] ATLAS Collaboration, *Performance of electron and photon triggers in ATLAS during LHC Run 2*, Eur. Phys. J. C **80** (2020) 47, arXiv: 1909.00761 [hep-ex] (cit. on p. 3).

[27] ATLAS Collaboration, *Prompt and non-prompt* J/ψ *and* $\psi(2S)$ *suppression at high transverse momentum in* 5.02 *TeV Pb+Pb collisions with the ATLAS experiment*, Eur. Phys. J. C **78** (2018) 762, arXiv: 1805.04077 [hep-ex] (cit. on pp. 3, 7).

[28] T. Sjöstrand, S. Mrenna and P. Skands, *A brief introduction to PYTHIA 8.1*, Comput. Phys. Commun. **178** (2008) 852, arXiv: 0710.3820 [hep-ph] (cit. on p. 4).

[29] ATLAS Collaboration, *ATLAS Pythia 8 tunes to* 7 *TeV data*, ATL-PHYS-PUB-2014-021, 2014, URL: https://cds.cern.ch/record/1966419 (cit. on p. 4).

[30] R. D. Ball et al., *Parton distributions with LHC data*, Nucl. Phys. B **867** (2013) 244, arXiv: 1207.1303 [hep-ph] (cit. on p. 4).

[31] E. Bothmann et al., *Event generation with Sherpa 2.2*, SciPost Phys. **7** (2019) 034, arXiv: 1905.09127 [hep-ph] (cit. on p. 4).

[32] F. Siegert, *A practical guide to event generation for prompt photon production with Sherpa*, J. Phys. G **44** (2017) 044007, arXiv: 1611.07226 [hep-ph] (cit. on p. 4).

[33] R. D. Ball et al., *Parton distributions for the LHC run II*, JHEP **04** (2015) 040, arXiv: 1410.8849 [hep-ph] (cit. on p. 4).

[34] J. Bellm et al., *Herwig 7.0/Herwig++ 3.0 release note*, Eur. Phys. J. C **76** (2016) 196, arXiv: 1512.01178 [hep-ph] (cit. on p. 4).

[35] L. Harland-Lang, A. Martin, P. Motylinski and R. Thorne, *Parton distributions in the LHC era: MMHT 2014 PDFs*, Eur. Phys. J. C **75** (2015) 204, arXiv: 1412.3989 [hep-ph] (cit. on p. 4).

[36] GEANT4 Collaboration, S. Agostinelli et al., *GEANT4 – a simulation toolkit*, Nucl. Instrum. Meth. A **506** (2003) 250 (cit. on p. 4).

[37] ATLAS Collaboration, *Electron and photon performance measurements with the ATLAS detector using the 2015–2017 LHC proton–proton collision data*, JINST **14** (2019) P12006, arXiv: 1908.00005 [hep-ex] (cit. on p. 5).

[38] ATLAS Collaboration, *Measurement of the jet radius and transverse momentum dependence of inclusive jet suppression in lead–lead collisions at $\sqrt{s_{NN}} = 2.76$ TeV with the ATLAS detector*, Phys. Lett. B **719** (2013) 220, arXiv: 1208.1967 [hep-ex] (cit. on p. 5).

[39] ATLAS Collaboration, *Measurement of the photon identification efficiencies with the ATLAS detector using LHC Run 2 data collected in 2015 and 2016*, Eur. Phys. J. C **79** (2019) 205, arXiv: 1810.05087 [hep-ex] (cit. on pp. 5, 6).

[40] M. Cacciari, G. P. Salam and G. Soyez, *The anti-k_t jet clustering algorithm*, JHEP **04** (2008) 063, arXiv: 0802.1189 [hep-ph] (cit. on p. 5).

[41] M. Cacciari, G. P. Salam and G. Soyez, *FastJet user manual*, Eur. Phys. J. C **72** (2012) 1896, arXiv: 1111.6097 [hep-ph] (cit. on p. 5).

[42] ATLAS Collaboration, *Jet energy measurement and its systematic uncertainty in proton–proton collisions at $\sqrt{s} = 7$ TeV with the ATLAS detector*, Eur. Phys. J. C **75** (2015) 17, arXiv: 1406.0076 [hep-ex] (cit. on p. 5).

[43] ATLAS Collaboration, *Jet energy scale and its uncertainty for jets reconstructed using the ATLAS heavy ion jet algorithm*, ATLAS-CONF-2015-016, 2015, URL: https://cds.cern.ch/record/2008677 (cit. on pp. 5–7).

[44] ATLAS Collaboration, *Measurement of the inclusive isolated prompt photon cross section in pp collisions at $\sqrt{s} = 8$ TeV with the ATLAS detector*, JHEP **08** (2016) 005, arXiv: 1605.03495 [hep-ex] (cit. on p. 6).

[45] ATLAS Collaboration, *Measurement of the cross section for inclusive isolated-photon production in pp collisions at $\sqrt{s} = 13$ TeV using the ATLAS detector*, Phys. Lett. B **770** (2017) 473, arXiv: 1701.06882 [hep-ex] (cit. on p. 6).

[46] ATLAS Collaboration, *Measurement of the inclusive isolated prompt photons cross section in pp collisions at $\sqrt{s} = 7$ TeV with the ATLAS detector using $4.6\,fb^{-1}$*, Phys. Rev. D **89** (2014) 052004, arXiv: 1311.1440 [hep-ex] (cit. on p. 6).

[47] ATLAS Collaboration, *High-E_T isolated-photon plus jets production in pp collisions at $\sqrt{s} = 8$ TeV with the ATLAS detector*, Nucl. Phys. B **918** (2017) 257, arXiv: 1611.06586 [hep-ex] (cit. on p. 6).

[48] G. D'Agostini, *A Multidimensional unfolding method based on Bayes' theorem*, Nucl. Instrum. Meth. A **362** (1995) 487 (cit. on p. 6).

[49] T. Adye, 'Unfolding algorithms and tests using RooUnfold', *Proceedings, 2011 Workshop on Statistical Issues Related to Discovery Claims in Search Experiments and Unfolding (PHYSTAT 2011)* (CERN, Geneva, Switzerland, 17th–20th Jan. 2011) 313, arXiv: 1105.1160 [physics.data-an] (cit. on p. 6).

[50] ATLAS Collaboration, *Electron and photon energy calibration with the ATLAS detector using 2015–2016 LHC proton–proton collision data*, JINST **14** (2019) P03017, arXiv: 1812.03848 [hep-ex] (cit. on p. 6).

[51] ATLAS Collaboration, *Measurement of jet fragmentation in Pb+Pb and pp collisions at* $\sqrt{s_{NN}} = 5.02$ *TeV with the ATLAS detector*, Phys. Rev. C **98** (2018) 024908, arXiv: 1805.05424 [hep-ex] (cit. on p. 6).

[52] ATLAS Collaboration, *Measurements of azimuthal anisotropies of jet production in Pb+Pb collisions at* $\sqrt{s_{NN}} = 5.02$ *TeV with the ATLAS detector*, (2021), arXiv: 2111.06606 [nucl-ex] (cit. on p. 6).

[53] ATLAS Collaboration, *Jet energy measurement with the ATLAS detector in proton–proton collisions at* $\sqrt{s} = 7$ *TeV*, Eur. Phys. J. C **73** (2013) 2304, arXiv: 1112.6426 [hep-ex] (cit. on p. 6).

[54] ATLAS Collaboration, *Jet energy scale measurements and their systematic uncertainties in proton–proton collisions at* $\sqrt{s} = 13$ *TeV with the ATLAS detector*, Phys. Rev. D **96** (2017) 072002, arXiv: 1703.09665 [hep-ex] (cit. on p. 6).

[55] ATLAS Collaboration, *Jet energy resolution in proton–proton collisions at* $\sqrt{s} = 7$ *TeV recorded in 2010 with the ATLAS detector*, Eur. Phys. J. C **73** (2013) 2306, arXiv: 1210.6210 [hep-ex] (cit. on p. 7).

[56] ATLAS Collaboration, *Determination of jet calibration and energy resolution in proton–proton collisions at* $\sqrt{s} = 8$ *TeV using the ATLAS detector*, Eur. Phys. J. C **80** (2020) 1104, arXiv: 1910.04482 [hep-ex] (cit. on p. 7).

[57] ATLAS Collaboration, *Luminosity determination in pp collisions at* $\sqrt{s} = 8$ *TeV using the ATLAS detector at the LHC*, Eur. Phys. J. C **76** (2016) 653, arXiv: 1608.03953 [hep-ex] (cit. on p. 7).

[58] ATLAS Collaboration, *Dynamics of isolated-photon plus jet production in pp collisions at* $\sqrt{s} = 7$ *TeV with the ATLAS detector*, Nucl. Phys. B **875** (2013) 483, arXiv: 1307.6795 [hep-ex] (cit. on p. 7).

[59] F. Arleo, K. J. Eskola, H. Paukkunen and C. A. Salgado, *Inclusive prompt photon production in nuclear collisions at RHIC and LHC*, JHEP **04** (2011) 055, arXiv: 1103.1471 [hep-ph] (cit. on p. 9).

[60] ATLAS Collaboration, *Measurement of prompt photon production in* $\sqrt{s_{NN}} = 8.16$ *TeV p+Pb collisions with ATLAS*, Phys. Lett. B **796** (2019) 230, arXiv: 1903.02209 [hep-ex] (cit. on p. 9).

[61] ATLAS Collaboration, *Measurement of* $W^{\pm}$ *boson production in Pb+Pb collisions at* $\sqrt{s_{NN}} = 5.02$ *TeV with the ATLAS detector*, Eur. Phys. J. C **79** (2019) 935, arXiv: 1907.10414 [hep-ex] (cit. on p. 9).

[62] R. Kunnawalkam Elayavalli and K. C. Zapp,
Simulating V+jet processes in heavy ion collisions with JEWEL, Eur. Phys. J. C **76** (2016) 695,
arXiv: 1608.03099 [hep-ph] (cit. on p. 11).